

An Infrared Study of OCS Binding and Size-selective Reactivity with Gold Clusters, Au_n^+ ($n = 1-10$)

*Alice E. Green,¹ Sascha Schaller,² Gabriele Meizyte,¹ Benjamin J. Rhodes,¹ Sean P. Kealy,¹
Alexander S. Gentleman,¹ Wieland Schöllkopf,² André Fielicke,^{2,3} Stuart R. Mackenzie^{1*}*

¹ Department of Chemistry, University of Oxford, Physical and Theoretical Chemistry Laboratory, South Parks Road, Oxford, United Kingdom, OX1 3QZ

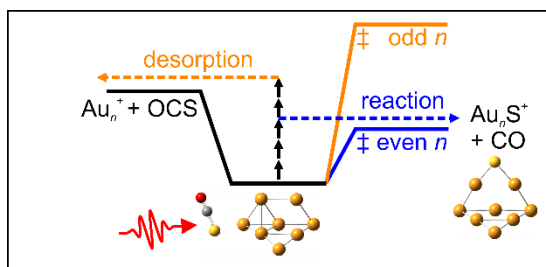
² Fritz-Haber-Institut der Max-Planck-Gesellschaft, Faradayweg 4-6, 14195 Berlin, Germany

³ Institut für Optik und Atomare Physik, Technische Universität Berlin, Hardenbergstraße 36, 10623 Berlin

*stuart.mackenzie@chem.ox.ac.uk

ABSTRACT

OCS binding to and reactivity with isolated gold cluster cations, Au_n^+ ($n = 1-10$) has been studied by infrared multiple photon dissociation (IR-MPD) spectroscopy in conjunction with quantum chemical calculations. The distribution of complexes $\text{Au}_n\text{S}_x(\text{OCS})_m^+$ formed reflects the relative reactivity of different cluster sizes with OCS, under the multiple collision conditions of our ablation source. The IR-MPD spectra of $\text{Au}_n(\text{OCS})^+$ ($n = 3-10$) clusters are interpreted in terms of either μ^1 or μ^2 S- binding motifs. Analysis of the fragmentation products following infrared excitation of parent $\text{Au}_n(\text{OCS})^+$ clusters reveals strongly size-selective (odd-even) branching ratios for OCS and CO loss, respectively. CO loss signifies infrared-driven OCS decomposition on the cluster surface and is observed to occur predominantly on even n clusters (*i.e.*, those with odd electron counts). The experimental data, including fragmentation branching ratios, are consistent with calculated potential energy landscapes, in which the initial species trapped are molecularly-bound entrance channel complexes, rather than global minimum inserted structures. Attempts to generate $\text{Rh}_n(\text{OCS})^+$ and $\text{Pt}_n(\text{OCS})^+$ equivalents failed; only sulfide reaction products were observed in the mass spectrum, even after cooling the cluster source to -100°C .



1. Introduction

In marked contrast to its inert bulk state, nanoscale gold exhibits pronounced and selective catalytic activity under mild conditions.¹⁻³ The increased reactivity of small gold particles is understood to arise from relativistic effects leading to the *d*-band lying higher in energy than for bulk gold.⁴⁻⁶ As such, small gold clusters and nanoparticles have found application in reactions as diverse as CO oxidation, epoxidation, nitric oxide reduction, alcohol synthesis, the water gas shift reaction, air purification and water splitting.^{1-2, 7-13} Gold has a famously strong bond with sulfur, and alkanethiols and disulfides at gold surfaces have received much attention,¹⁴⁻¹⁶ as has the protection of gold clusters using thiolates.¹⁷ These serve to stabilise gold nanoparticles, preventing their coalescence, and find applications ranging from drug delivery, to enantiospecific catalysis, and the semiconductor industry.¹⁵⁻¹⁸ Accordingly, the study of the Au-S interaction and binding motifs such as sulfur bridges have been crucial to the development of this field.¹⁹

Key features in determining the activity of a gold particle are its size and charge with the latter dependent on the nature of any support.^{3, 8-9, 20-24} The exact particle size can have a profound effect on catalytic activity and many studies have attempted to identify the perfect nanocatalyst size and structure for a particular application.^{23, 25} These catalysts can range from a few atoms – Au₈ clusters are particularly active in CO oxidation²⁶⁻²⁷ – to several nanometers.³

The ability to accept and donate electrons is central to catalytic function and thus controlling the charge on a catalytic particle is also important. This can be done using a catalyst support and / or spectator ligands.^{8-9, 12, 24} For example, partial electron transfer from a MgO support plays a key role in the activity of the Au₈ catalyst.²⁶⁻²⁷ Surface X-ray absorption studies of CO oxidation on

gold clusters have revealed optimum activity when 60% of gold is positively charged,²⁸⁻³⁰ and trace water levels can perturb the electron density on a gold catalyst particle enhancing its reactivity.¹²

Gas-phase cluster studies can achieve exquisite control of both cluster size and charge state. Mass spectrometry techniques permit the study of trends in reactivity and charge characteristics, which may guide target properties for deposited particles.³¹⁻³³ Such fundamental studies, using a range of techniques,³⁴⁻³⁶ including ion mobility,³⁷⁻³⁹ and visible photodissociation spectroscopy,⁴⁰ continue to reveal unique physico-chemical features in gold clusters, $\text{Au}_n^{+/0/-}$, such as the transformation from planar to three-dimensional ground state structures at surprisingly large cluster sizes ($n = 8, 11, 12$ for cations, neutrals, and anions, respectively) – another result arising from relativistic effects. These and other investigations of $\text{Au}_n^{+/0/-}$ clusters often reveal oscillating trends with increasing cluster size, n , in properties including cluster stability, dissociation energy, ionisation potential, electron affinity, fragmentation pathways and HOMO-LUMO gap.^{20, 41-48}

Due to the electronic structure of gold, the cluster size, n , and charge effects are very closely linked,⁴⁹ and many observations have been interpreted in terms of electron counting models in which each gold atom, with the $[\text{Xe}]4f^{14}5d^{10}6s^1$ configuration, is considered as monovalent, similar to alkali metals.^{20, 50} Within such jellium models,⁵¹ gold clusters exhibit electronic shell structures with magic numbers corresponding to shell closures at 8, 18, 20, *etc.*⁵²⁻⁵³ Similarly, oscillating odd-even effects in the size-dependence of many gold cluster properties are explained by electron pairing with every other cluster size having odd numbers of electrons, *i.e.*, Au_n^0 ($n = \text{odd}$) or $\text{Au}_n^{+/-}$ ($n = \text{even}$).

Vibrational spectroscopy provides an ideal tool with which to explore molecular activation on metal clusters *via* red-shifts in adsorbate stretching frequencies. On gold clusters, these spectral shifts and the activation they reflect, often exhibit odd-even oscillations. Along with other techniques,⁵⁴⁻⁶² infrared multiple photon dissociation (IR-MPD) studies of O₂ binding to Au_{*n*}^{+/-} have revealed that O₂ binds only to even *n* anion clusters,⁶³ to Au_{*n*}⁺ cations with low 2nd ionisation energies (e.g., Au₁₀⁺ and Au₂₂⁺),⁶⁴ and O₂ is more activated by odd than even *n* neutral clusters.⁶⁵ The NO stretching frequency of Au_{*n*}NO⁺ complexes exhibits marked odd-even alternation, as the unpaired electron in the 1 Au_{*n*}⁺ (*n* = even) clusters efficiently donates into the NO π* orbital, efficiently activating it.⁷

Infrared studies of other adsorbates (e.g., CO,^{7, 66} methane,⁶⁷ methanol,⁶⁸⁻⁷⁰ ethanol,⁷¹ and ethene⁷²) on gold clusters suggest alternative binding mechanisms for which odd-even size effects are less clear. All small gold clusters selectively dissociate a single C–H bond in CH₄ but, whilst CH₄ binding energies to Au_{*n*}⁺ show a clear size dependence,⁷³ this is not reflected in the IR-MPD spectra.⁶⁷ Infrared action spectroscopy has also been used extensively to study Au⁺–L_{*m*} (L = N₂O, CO, NO, H₂O, and small hydrocarbons) metal-ligand complexes.⁷⁴⁻⁷⁹

When radical species such as OH are preadsorbed onto gold cluster anions the odd-even pattern in cluster reactivity reverses, accounting for the role of water in the enhanced activity of some nano gold catalysts.¹² Indeed, the binding of one molecule to a cluster can have a profound effect on the subsequent adsorption of a second molecule. Coadsorption of H₂, for example, enhances O₂ binding to Au_{*n*}⁺,⁶² and the presence of CO promotes O₂ binding to otherwise unreactive Au_{*n*}⁻, leading to CO₂ formation.⁸⁰⁻⁸³

In guided ion beam experiments of metal monomer cations (M^+) with OCS, Armentrout and coworkers,⁸⁴⁻⁸⁹ found MS^+ to be the dominant reaction product following insertion elimination. Bohme and coworkers, by contrast, showed that under single collision conditions OCS binds molecularly to Au^+ , without AuS^+ formation.⁹⁰

Here, we present an infrared spectroscopic study of OCS binding to gas-phase gold clusters. Carbonyl sulfide is an important sulfur transfer reagent in the hydrodesulfurisation of natural gas,⁹¹⁻⁹² and OCS interaction, activation and reactivity with extended metal surfaces have been extensively studied.⁹³ OCS also represents an intrinsically interesting adsorbate / reactant in that a range of different potential binding motifs to gold clusters are possible. OCS denotes an analogue of CO_2 but S- and O-bound structures can lead to differential activation in a similar way to N- and O- binding of N_2O .^{74, 94} CO_2 , N_2O and OCS are isoelectronic 16 valence electron systems,⁹⁵⁻⁹⁷ and may be activated either by withdrawing electron density from the strongly-bonding HOMO or by electron donation into the antibonding π^* LUMO. CO_2 binding to cations suggests weak activation by the former,⁹⁸⁻¹⁰² but anionic clusters can lead to extensive CO_2 bending / activation by donation into the LUMO,¹⁰³ (see, for example, $[Pt_4CO_2]^-$).¹⁰⁴ Activation of OCS on metal clusters thus depends on the electron density of the cluster and its ability to donate or withdraw electron density.

Here, we describe a detailed free electron laser IR-MPD study designed to understand the binding of OCS to cationic gold clusters, Au_n^+ ($n = 1-10$). Gold clusters are generated by laser ablation, exposed to low pressure OCS under thermalising multiple collision conditions, and the species produced subject to intense infrared tuneable radiation from a free electron laser. The resulting IR-MPD spectra reveal details of the interactions involved as well as cluster size-dependent reaction pathways.

2. Experimental and Computational Methods

The instrument and IR source used in these studies have been described in detail previously.¹⁰⁴⁻¹⁰⁷ Briefly, gold cluster cations are generated by pulsed laser ablation of a gold target in the presence of He carrier gas within a cluster source maintained at *ca.* 30°C. Low pressure OCS is introduced to a reaction channel ~40 mm downstream from the ablation point. The clusters undergo multiple thermal collisions with OCS and He prior to expansion into vacuum, forming a cluster beam. The resulting distribution of cationic species is probed by reflectron time of flight mass spectrometry. The whole experiment operates at 10 Hz and mass-resolved IR-MPD spectra are recorded by subjecting alternate cluster pulses to the output of the FHI infrared free electron laser,¹⁰⁵ (operating 350-2300 cm⁻¹). IR-MPD spectra are recorded by evaluating the fractional depletion of the parent ion signal, as a function of infrared wavenumber.

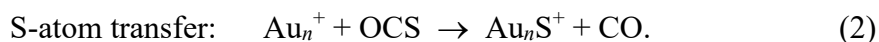
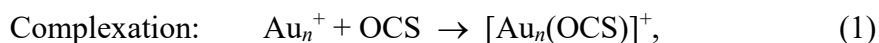
In order to help interpret the experimental spectra, we have performed a DFT study of energetically low-lying structural isomers of relevant species in different spin states. The Au_{*n*}⁺, and subsequently, Au_{*n*}(OCS)⁺ structure search was performed using a large range of chemically intuitive starting structures, in addition to the stochastic KICK algorithm developed by Addicoat and Metha.¹⁰⁸ The search for the Au_{*n*}⁺ geometries included structures determined by ion mobility measurements.³⁸ A range of functionals and basis sets was employed, with comparisons shown below for the representative UB3P86-SDD,¹⁰⁹ functional-basis set combination. Scalar relativistic effects were included via the use of the Stuttgart Dresden effective core potential (ECP60 for gold atoms).¹¹⁰ Use of the TPSS functional,¹¹¹ and, Def2TZVP,¹¹²⁻¹¹³ basis set, and further inclusion of dispersion parameters,¹¹⁴⁻¹¹⁵ made no qualitative difference to the relative energy ordering of key structures. To aid comparison with experiment, calculated frequencies have been scaled by a factor

of 1.039 to match the known frequency of the C=S stretch in free OCS.¹¹⁶ All calculations were performed using the Gaussian09 suite of programs.¹¹⁷ The supporting information contains further details of the computational methods and results.

3. Results and Discussion

3.1 Mass spectra and $\text{Au}_n^+ + \text{OCS}$ reactivity

Figure 1 shows the mass spectrum of species produced by the ablation of a gold target in the presence of low pressure OCS introduced via the late mixing valve. Conditions were optimised to generate clusters in the size range Au_n^+ ($n=1-15$) and a range of OCS complexes and other reaction products are observed. Two net processes dominate the initial product species identified in the mass spectra:



The latter may be direct, or more likely, decomposition following process (1). There is no evidence in the mass spectrum for the conceivable O-atom transfer reaction:



nor is there evidence for production of $\text{Au}_n(\text{CO})^+$, $\text{Au}_n(\text{CS})^+$, or $\text{Au}_n(\text{SO})^+$. The prevalence of S-atom transfer over O-atom transfer reflects the relative C=O and C=S bond strengths of OCS (6.51 eV and 3.22 eV, respectively), which in turn determines the height of the transition state for reactivity.¹¹⁸

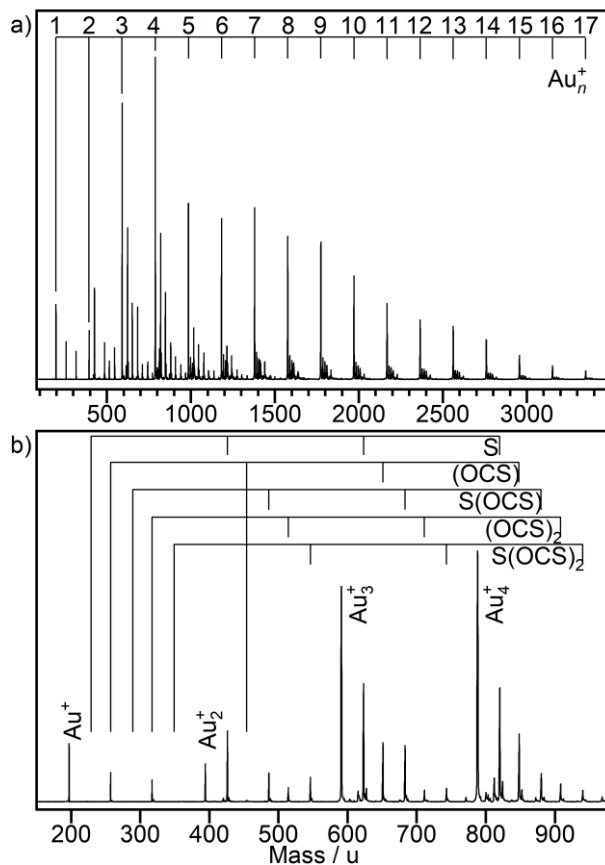


Figure 1. a) Representative time of flight mass spectrum obtained following laser ablation of a gold target in the presence of a carrier gas of helium and reaction gas of OCS. b) An enlarged section of a) illustrating size-dependent reactivity for the smallest clusters.

In similar experiments performed with Pt_n^+ ($n \leq 15$) and Rh_n^+ ($n \leq 25$) clusters, no $[\text{M}_n(\text{OCS})]^+$ complexes were observed, with all clusters in this size range reacting readily to form sulfides, M_nS_x^+ (see Figure S1, supporting information). Even under cooled (-100°C) cluster source conditions, no $[\text{M}_n(\text{OCS})]^+$ species were detected for $\text{M} = \text{Pt}, \text{Rh}$.

Under the multiple collision conditions employed here, it is clear from Figure 1b that the branching ratios of reactions (1) and (2) show marked size-dependence in the small size regime $n \leq 4$. Mass

spectra were measured at a wide range of backing pressures and OCS partial pressures, and Figure 1 is representative of the distributions obtained. Figure 2 summarises the relative intensities of species produced as a function of cluster size, n . In the case of the monomer cation, Au^+ , only sequential complexation is observed resulting in $[\text{Au}(\text{OCS})_m]^+$ species (the square brackets reflecting that these are empirical formulae only, and no information on the nature of the adsorption, molecular *versus* dissociative, should be inferred). These observations are consistent with the single collision experiments by Bohme and coworkers of a range of monomer cations,⁹⁰ in which PtS^+ was the sole product of $\text{Pt}^+ + \text{OCS}$ reactions, but no AuS^+ was observed in reaction of Au^+ . By contrast, for reactions of Au_n^+ ($2 \leq n \leq 8$) + OCS, the sulfide represents a major reaction product (blue and green columns in Figure 2).

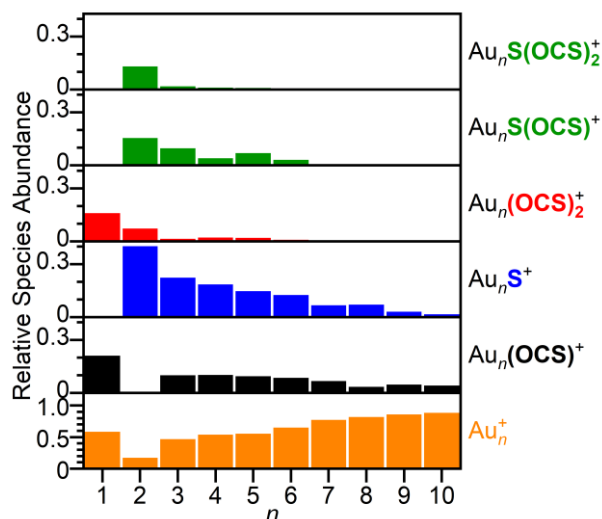


Figure 2. Relative species abundance of the major $\text{Au}_n\text{S}_x(\text{OCS})_m^+$ ($n = 1-10$, $m = 0-2$, $x = 0, 1$) species produced in the cluster beam by ablation of a gold target with OCS introduced downstream. Although shown for the individual conditions employed in Figure 1, these distributions are representative of all OCS pressures employed. The relative abundance is determined from the time of flight spectrum as the integrated area of each Au_nX^+ signal as a fraction of the area of all X species for each n .

The final Au_2^+ signal itself is anomalously weak – in part reflecting the efficiency of the S-atom transfer reaction. However, the $[\text{Au}_2(\text{OCS})_2]^+$ signal suggests $[\text{Au}_2(\text{OCS})]^+$ exists as a highly reactive intermediate, but is not easily stabilised by collision. With the notable exception of Au_2^+ , efficient $[\text{Au}_n(\text{OCS})]^+$ stabilisation occurs on all cluster sizes (black bars), and the branching ratio for process (1) increases relative to process (2), with increasing n , suggesting a smooth decrease in bond breaking (*i.e.*, Au_nS^+ forming) reactivity. For all cluster sizes $3 \leq n \leq 10$, the $[\text{Au}_n(\text{OCS})]^+$ signal is strong enough to record IR-MPD spectra (see section 3.2).

3.2 IR-MPD spectra of $\text{Au}_n(\text{OCS})^+$

Figure 3 shows the IR-MPD spectra of $[\text{Au}_n(\text{OCS})]^+$ ($n=3-10$) clusters. The spectra are similar for all cluster sizes, with clear features observed near 2100 cm^{-1} and 790 cm^{-1} and some evidence of a third feature around 500 cm^{-1} . These bands are readily interpreted as the fully-allowed fundamental bands of the OCS vibrational normal modes: the C=O stretch, the C=S stretch, and the bending modes, respectively, and their presence unambiguously identifies the OCS binding as molecular (*i.e.*, non dissociative).

Comparison of the observed band positions with those in free OCS (C=O stretch: 2062 cm^{-1} , C=S stretch: 859 cm^{-1} , bend: 520 cm^{-1}),¹¹⁶ give a clear indication of the nature of this binding. The C=S band in $\text{Au}_n(\text{OCS})^+$ is red-shifted by *ca.* 70 cm^{-1} (8%) relative to that in free OCS whilst the C=O band is weakly blue-shifted by *ca.* 40 cm^{-1} (2%), clearly indicating binding via the S-atom. This is consistent with the calculated structures and simulated spectra in Section 3.3, below, which show these entrance channel species to be bound predominantly by sigma donation from the bonding OCS HOMO, which is mainly located on the C=S bond (see Figure S12, supporting information).

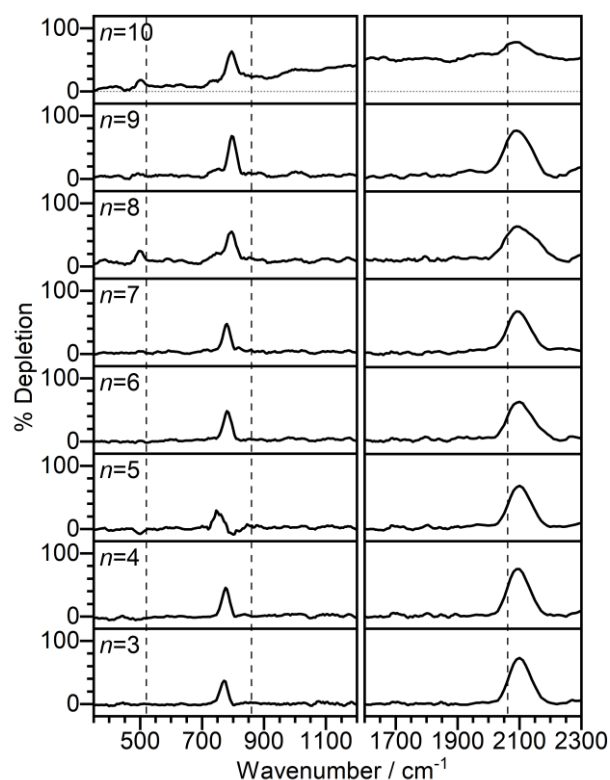


Figure 3. IR-MPD spectra of $\text{Au}_n(\text{OCS})^+$ ($n = 3-10$) clusters illustrating molecularly-adsorbed OCS. The dashed lines indicate the frequency of the bend (520 cm^{-1}), C=S stretch (859 cm^{-1}), and C=O stretch (2062 cm^{-1}) vibrations in free OCS.¹¹⁶

Only weak trends in the vibrational band positions with cluster size are observed. The 2100 cm^{-1} band is essentially static with cluster size, while the C=S stretch blue-shifts slightly from 770 cm^{-1} to 795 cm^{-1} between $n = 3$ and 10. Two other features in Figure 3 are worthy of note; Firstly, the $\text{Au}_{10}(\text{OCS})^+$ spectrum exhibits a broad non-zero background which extends from 700 cm^{-1} to 2300 cm^{-1} and beyond. This broad, reproducible signal, which will be the subject of a future publication in its own right, is not unique to $\text{Au}_{10}(\text{OCS})^+$ but has been observed in several other systems of closed shell ligands binding to Au_{10}^+ and we thus believe it to be an inherent feature of the Au_{10}^+ cluster – probably an anomalously low-lying electronic band. Secondly, the C=S stretch in the

$\text{Au}_5(\text{OCS})^+$ spectrum is red-shifted relative to the same band in other clusters and will be discussed in Section 3.3 below. For completeness, the corresponding spectra of the $\text{Au}_n\text{S}(\text{OCS})^+$ ($n = 2-6$) clusters are shown in Figure S4 in the supporting information and are analysed in the same way as $\text{Au}_n(\text{OCS})^+$ clusters.

3.3 Comparison with simulated spectra from DFT calculations

To confirm the assignments made above, the experimental $\text{Au}_n(\text{OCS})^+$ ($n = 3-10$) IR-MPD spectra have been compared with the simulated spectra of energetically low-lying structures from density functional theory. By way of example, Figure 4 shows both experimental and simulated spectra of $\text{Au}_8(\text{OCS})^+$. Calculations of other cluster sizes reveal qualitatively similar structures and simulated spectra (see Figures S6-S8, supporting information). All calculated structures shown in Figure 4 are doublet spin states, with higher multiplicities calculated to lie at least 1.97 eV higher in energy. All simulated spectra have been convoluted with a Lorentzian function with a 20 cm^{-1} full width half maximum to aid comparison with the experimental data.

The lowest energy structure calculated is an inserted $\text{SAu}_8(\text{CO})^+$ structure which lies much lower in energy than molecularly-bound structures. The presence of the C=O band in the same 2100 cm^{-1} spectral region as the OCS C=O stretch, renders this area useless for diagnostic purposes. The C=S stretching region ($\sim 790\text{ cm}^{-1}$), by contrast is much more useful since observation of the C=S stretching band is inconsistent with insertion into the C=S bond and thus the spectrum cannot be assigned to the lowest energy calculated structure. Isomers with insertion into the C=O bond of OCS lie at least 3.31 eV higher in energy than the lowest lying structure identified, so can be neglected. Hence, the spectrum in Figure 4 is assigned to molecularly-adsorbed OCS. For this

reason, the energies of the calculated structures are given relative to the lowest energy molecularly-bound structure.

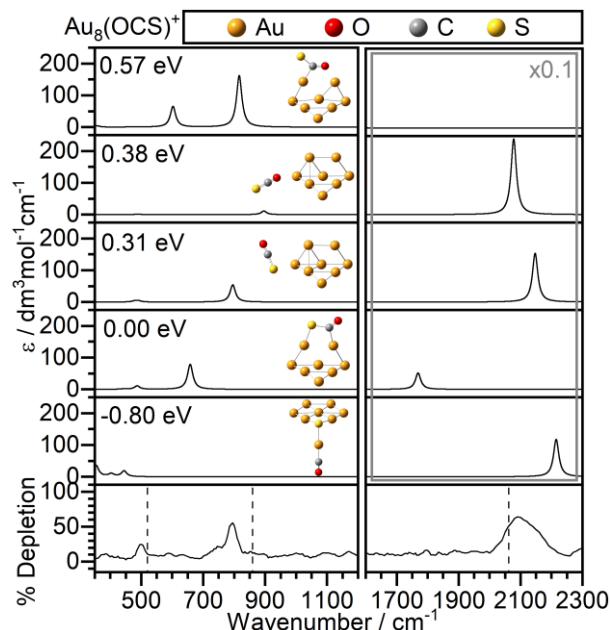


Figure 4. Comparison of the IR-MPD spectrum of $\text{Au}_8(\text{OCS})^+$ with simulated IR spectra for energetically low-lying isomers, all with a doublet spin state. Intensities are given as ϵ , the molar absorption coefficient. Energies are relative to the lowest molecularly-bound structure and are zero-point corrected. Other cluster sizes are in the supporting information.

In the lowest energy molecularly-bound structure of $\text{Au}_8(\text{OCS})^+$, the OCS is significantly activated as indicated by the markedly bent nature of the OCS, which is doubly-bound in a side-on fashion, similar to the structure of activated CO_2 on $[\text{Pt}_4]^-$.¹⁰⁴ The experimental spectrum, however, does not support this structure for which significant red-shifts in both stretching modes are predicted. Instead, the spectrum matches well with an isomer lying 0.31 eV higher in energy than the activated species. In this structure the OCS is S-bound, remains essentially linear and the vibrational bands are only weakly shifted from those in free OCS. This suggests that the complex remains trapped

in an entrance channel structure behind a significant reaction barrier to such activation, and much earlier on the reaction pathway than the dissociation barrier, resulting in the putative global minimum structure. All other $\text{Au}_n(\text{OCS})^+$ clusters studied can be similarly assigned to equivalent entrance channel species. There is little evidence of O-bound structures in any cluster studied here, unlike previous studies of N_2O on various small metal clusters.⁷⁴

The $\text{Au}_5(\text{OCS})^+$ cluster represents an interesting anomaly. The C=S stretch for this cluster is red-shifted relative to all other cluster sizes. Figure 5 shows this further activation can be explained by unique μ^2 -binding of the OCS, leading to additional withdrawal of electron density from the C=S π -bond. This bonding is facilitated by the uniquely flexible structure of the Au_5^+ planar bow tie structure. Figure 5b) shows that the μ^1 and μ^2 structures are almost isoenergetic and intrinsic reaction coordinate calculations find a low, 0.12 eV, barrier between the two. Both minima lie more than 0.75 eV below the $\text{Au}_5^+ + \text{OCS}$ asymptote. The negative signal at *ca.* 800 cm^{-1} suggests enhancement into this channel arising from fragmentation of larger clusters (such as $\text{Au}_5(\text{OCS})_2^+$), and thus we cannot rule out an additional (weak) μ^1 -bound structure. Two similarly low-lying minima were also observed in a DFT study of $\text{Au}_5^+(\text{C}_2\text{H}_6)$,¹¹⁹ and gold clusters are known to exhibit a wide range of low-lying structural isomers with low barriers to interconversion between cluster geometries.^{25, 37, 66}

Under the conditions employed here, multiple OCS molecules can bind to the smaller cluster sizes. $\text{Au}_n(\text{OCS})_m^+$ ($n; m = 3;3, 4;3, 4;4$) are also produced but are not observable on the scale of Figure 2. This introduces new features to the IR-MPD spectra as shown in Figure 6 for $\text{Au}_n(\text{OCS})_m^+$ ($n = 2-4; m = 1-4$) species. As more OCS molecules are adsorbed, the intensity of the bending mode ($\sim 500 \text{ cm}^{-1}$) increases with respect to that of the C=S-stretch. For $m = n$ clusters an additional band appears around 1000 cm^{-1} . Spectral simulations using the harmonic approximation are unable to

assign this band (see Figure S10, supporting information). The closest harmonic frequency is that of an O-bound OCS which is calculated to appear around 908 cm^{-1} . Instead, the new feature is assigned as an overtone / combination band arising from the linear combination of bending modes of individual OCS molecules. The vertical dashed lines in Figure 6 mark twice the value of the observed bending fundamental. The good overlap with the new feature and high intensity of the bending fundamental supports the overtone assignment. Spectral intensities in IR-MPD spectra must, however, be interpreted carefully. The OCS binding energy decreases with increasing m and each 1000 cm^{-1} photon delivers twice the energy of a 500 cm^{-1} photon and thus half the number of photons is required to drive fragmentation.

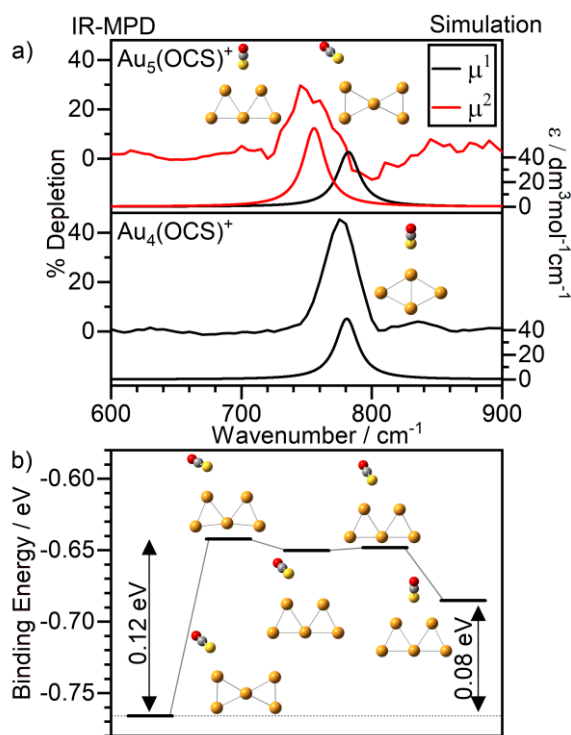


Figure 5. a) Comparison of the IR-MPD spectrum of $\text{Au}_4(\text{OCS})^+$ and $\text{Au}_5(\text{OCS})^+$ in the region of the C=S stretch, with simulated IR spectra for energetically low-lying isomers. Intensities are given as ϵ , the molar absorption coefficient. Uniquely for $\text{Au}_5(\text{OCS})^+$, we see evidence for μ^2 -bound OCS. Weak enhancement in the $\text{Au}_5(\text{OCS})^+$ signal around 800 cm^{-1} probably arises from depletion into this channel from $\text{Au}_5(\text{OCS})_2^+$. b) Calculated barrier height for the transition from μ^1 OCS binding to μ^2 .

The anharmonic frequency calculation of $\text{Au}_2(\text{OCS})_2^+$ in Figure 6 shows that the band can be assigned to combination bands of the in phase ($^+$) and out of phase ($^-$) bending modes of the two ligands. The calculated intensity ratio of the band fundamental to the combination band is similar to that observed experimentally. $\text{Au}_2(\text{OCS})_2^+$ is planar, and the OCS ligands can bend both in plane and out of plane. In phase combinations of both give rise to IR active bands, with displacement vectors given as $B1^+$ and $B2^+$ in Figure 6b), respectively. The corresponding out of phase versions are IR inactive ($B1^-$ and $B2^-$), but anharmonicity can couple them with their IR active counterparts to generate combination bands $B1^{+, -}$ and $B2^{+, -}$, very close in energy to the $B1^+$ and $B2^+$ overtones. For $m = 1$ species no such combination bands exist, only overtones and the bands in the spectra are accordingly weak.

The reason for the apparent absence of the S-bound C=S stretch for the $\text{Au}_4(\text{OCS})_4^+$ structure is unclear. For clusters $n > 4$, a maximum of one or two OCS molecules are observed to bind under the conditions employed here.

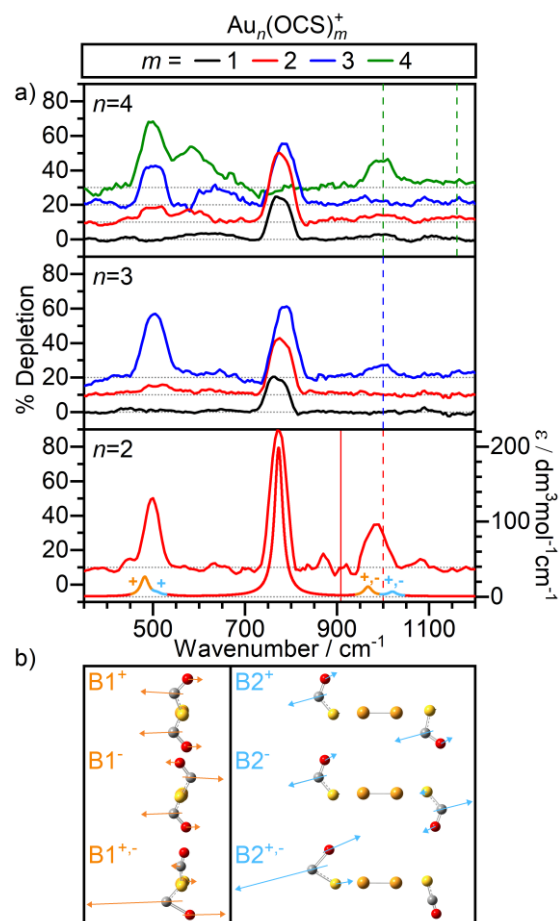
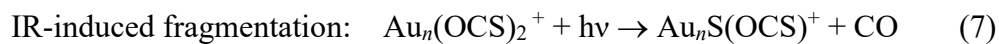
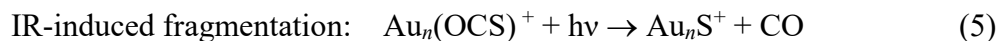


Figure 6. a) IR-MPD spectra illustrating an additional band present for $\text{Au}_n(\text{OCS})_m^+$ species where $m = n$, along with the anharmonic simulated spectrum for the S-bound entrance channel $\text{Au}_2(\text{OCS})_2^+$ cluster. b) B1^+ and B1^- correspond to the out of plane OCS bends which are, in phase and out of phase, respectively, and $+, -$ signifies a linear combination of the two. Similarly, B2^+ and B2^- correspond to the in plane OCS bends. The dashed lines in a) are positioned at twice the experimental bending frequency of all cluster sizes and the solid red vertical line indicates the calculated frequency for an O-bound OCS in $\text{Au}_2(\text{OCS})_2^+$.

3.4 Size-selective IR-induced bond breaking

The IR-MPD spectra of $\text{Au}_n(\text{OCS})^+$ clusters provide good evidence of kinetically-trapped entrance channel complexes. For every depletion signal observed in the IR-MPD spectrum of a parent ion,

a corresponding enhancement must be observed in some daughter fragment mass channel. The fragment lost upon IR absorption provides important information on the reaction pathway and the relative height of potential barriers and dissociation thresholds.^{94, 104, 120-123} For the species observed here, plausible fragmentation pathways include:



Given that the spectroscopy indicates only molecularly-adsorbed OCS, CO loss channels provide a clear signature of IR-induced OCS fragmentation. Figure 7 gives two example systems, $\text{Au}_2\text{S}_x(\text{OCS})_m^+$ and $\text{Au}_6\text{S}_x(\text{OCS})_m^+$, which illustrate the challenge of matching depletions with corresponding enhancements. In some cases, unambiguous matching proves impossible but in other cases, convincing conclusions can be drawn. For example, enhancement in the $\text{Au}_2\text{S}(\text{OCS})^+$ channel between 350 cm^{-1} and 1200 cm^{-1} is a likely signature of IR-driven OCS decomposition in $\text{Au}_2(\text{OCS})_2^+$, though some OCS loss from $\text{Au}_2\text{S}(\text{OCS})_2^+$ cannot be ruled out.

For larger clusters, such as $n = 6$, the pathways are less complex as fewer multiply decorated clusters are produced. It is clear in Figure 7b) that most Au_6S^+ production arises from IR-driven CO loss from $\text{Au}_6(\text{OCS})^+$ signifying IR-induced fragmentation. The similar enhancements

observed in both the Au_6^+ and Au_6S^+ reflect comparable branching ratios for processes (4) and (5), suggesting that the transition state to OCS dissociation on this cluster lies at an energy comparable with the $\text{Au}_6^+ + \text{OCS}$ dissociation threshold.

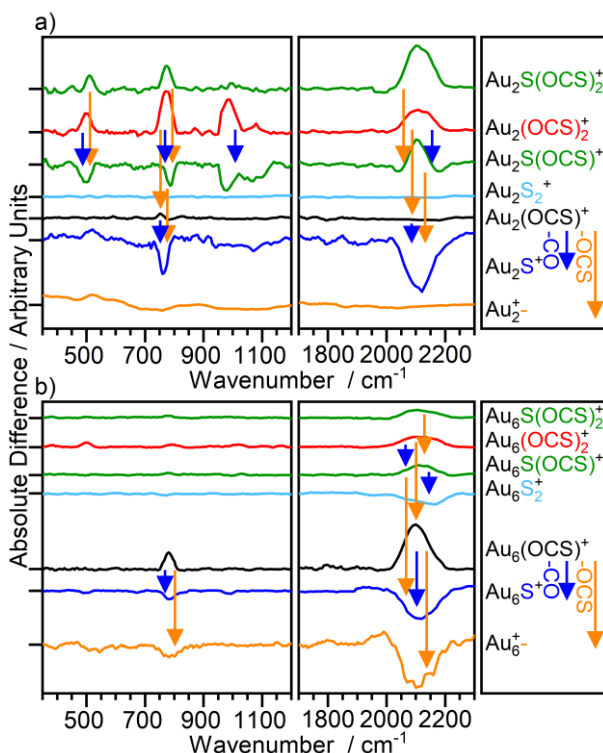


Figure 7. IR-MPD spectra of $\text{Au}_n\text{S}_x(\text{OCS})_m^+$ ($m = 0-2$, $x = 0-2$), a) $n = 2$ and b) $n = 6$, plotted as absolute difference (infrared on - infrared off), with depletion plotted in the positive direction. These example sizes illustrate the range of possible combinations of desorption pathways, indicated by the arrows. The blue arrow is depletion by loss of CO and the orange arrow is loss of OCS.

Figure 8 shows the IR-MPD spectra for $\text{Au}_n(\text{OCS})^+$ ($n = 2-10$) and related species in the region of the C=S stretch. Bare Au_3^+ and Au_4^+ spectra have not been given as the mass signal is too large to measure reliably signal enhancements in these channels. Colored arrows indicate either unambiguous OCS loss (process (4), orange arrows) or CO loss (process (5), blue arrows). A notable odd-even alternation is observed in the relative branching ratios for the two processes. For

even n $\text{Au}_n(\text{OCS})^+$ species, IR absorption tips the system over the dissociation barrier to completion, leading to efficient CO loss. Of particular note, $n = 8$ exhibits almost exclusive CO loss. By contrast, for odd n the dominant process is OCS loss, the branching ratio for which is close to unity for $n = 5, 7$ and 9 . This represents the first evidence of odd-even size-selective infrared-induced chemistry in metal cluster systems.

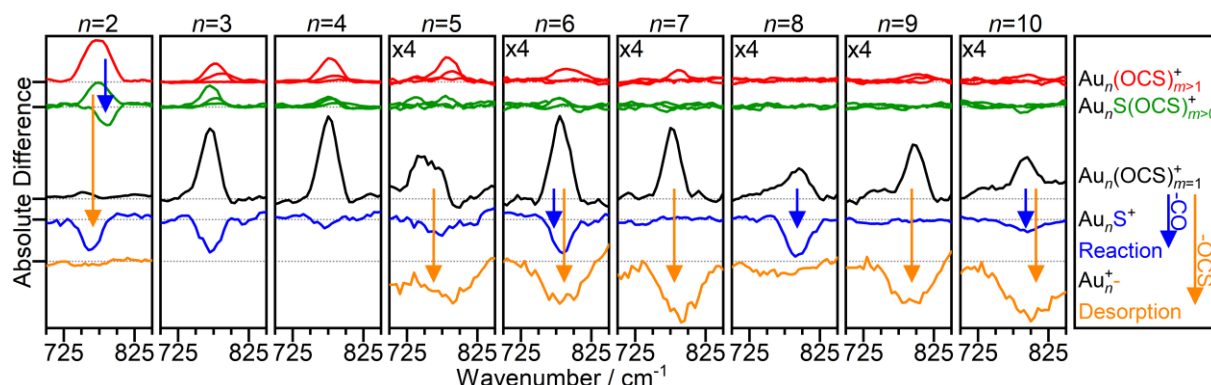


Figure 8. IR-MPD spectra of $\text{Au}_n\text{S}_x(\text{OCS})_m^+$ ($n = 2-10$, $m = 0-4$, $x = 0, 1$) clusters plotted as absolute difference (infrared on - infrared off, depletion plotted in the positive direction) in the region of the C=S stretch. Desorption pathways of $\text{Au}_n(\text{OCS})^+$ are indicated by the arrows. The other spectral regions can be found in the supporting information and are qualitatively similar. Bare Au_3^+ and Au_4^+ enhancements have not been given as the ion signal is too large to measure small enhancements reliably.

The key reactivity (*i.e.*, IR-driven CO loss) information in Figure 8 is collated in Figure 9, together with similar information in the region of the other OCS vibrations. Here, the reactivity is quantified as a ratio of the integrated Au_nS_x^+ enhancement to the depletion of the $\text{Au}_n(\text{OCS})_m^+$ parent, corrected for simple ligand loss from $\text{Au}_n\text{S}_x(\text{OCS})_m^+$ (process 8):

$$\text{Reactivity: } \frac{\sum_x \text{Au}_n \text{S}_x^+ - \sum_m \text{Au}_n \text{S}(\text{OCS})_m^+}{\sum_m \text{Au}_n (\text{OCS})_m^+}.$$

Overall, analysis of the bend and C=O stretch regions give similar results to that of the C=S stretch region (Figure S5, supporting information) with branching ratios of C=S bond breaking higher for even clusters than for adjacent odd clusters, reflecting the radical (unpaired electron) character) of the former. The bending region data must be treated with caution due to the small depletions which result in limited signal to noise.

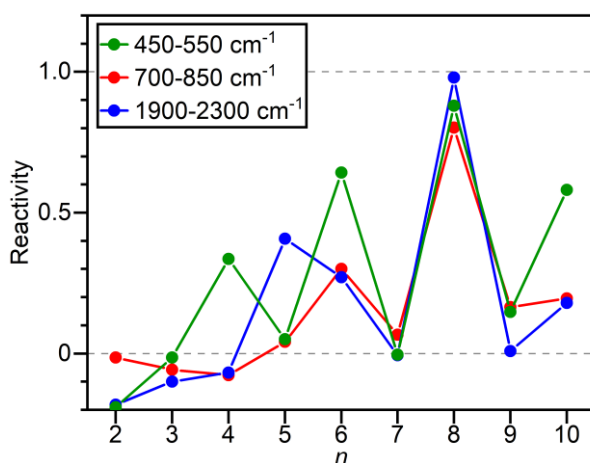


Figure 9. IR-induced reactivity, measured as a ratio of integrals of the spectra in Figure 8 and equivalent for the other two bands in the supporting information. Specifically, the enhancement into the sulfide clusters, $Au_nS_{1,2}^+$ as a fraction of $Au_n(OCS)_m^+$ depletion, correcting for sulfide enhancement from the depletion of $Au_nS(OCS)_m^+$ clusters.

The Au_5^+ series shows some divergence from the general picture, with Figure S5 in the supporting information showing much larger enhancements observed in the Au_5S^+ and $Au_5S_2^+$ channels following excitation in the 2100 cm^{-1} region. This is explained by the $Au_nS(OCS)^+$ depletion spectra in Figure 8 (see also Figures S4 and S5, supporting information), which reflects the different OCS binding for $Au_5S(OCS)^+$. The absence of the C=S stretch band for this cluster may indicate dissociative adsorption of OCS, in which case the observed 2100 cm^{-1} band arises from the C=O stretch in $Au_5S_2(CO)^+$.

3.5 Simulated reaction pathway and proposed mechanism

The IR-MPD spectra and the fragmentation branching ratios yield important information on the relevant reactive potential energy surface, a key part of which is shown in Figure 10 for $\text{Au}_{8,9}^+ + \text{OCS}$ calculated at the B3P86-SDD level. Three relevant potential minima are observed along the reaction pathway: an S-bound entrance channel complex, an activated species with distorted OCS structure, and an inserted putative global minimum structure. The calculated pathways agree well with the assignment of entrance channel complexes in the discussion of Figure 3 and 4; multiple collision conditions enable clusters to be trapped behind TS1.

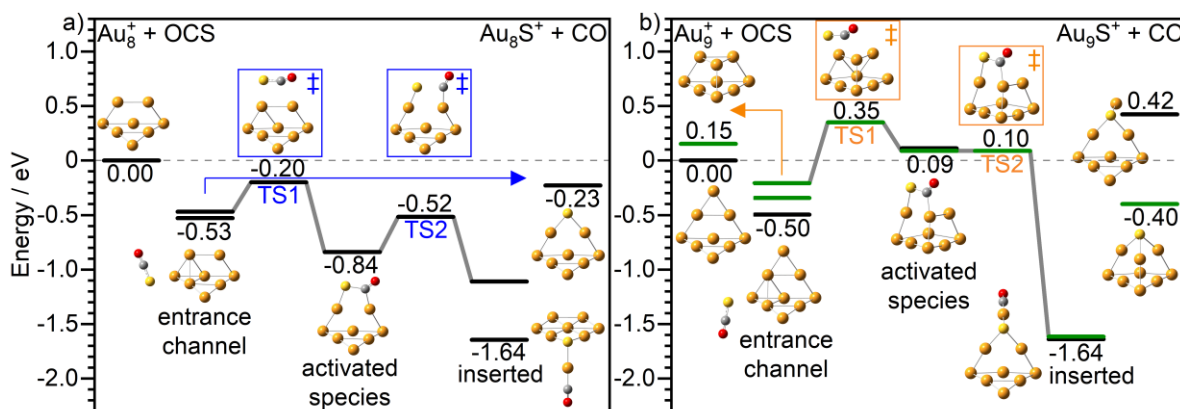


Figure 10. The key part of the potential energy surfaces for the dissociation of OCS on: a) Au_8^+ ($2S+1 = 2$), and b) Au_9^+ ($2S+1 = 1$), calculated at the B3P86-SDD level of theory. Geometries given are the lowest energy of each type and energies are relative to the $\text{Au}_n^+ + \text{OCS}$ asymptote. The green levels in b) indicate clusters based on a different Au_9^+ isomeric structure, which correlate with the lowest energy Au_9^+S product.

The reactive potential energy surface in Figure 10 also agrees qualitatively with the fragmentation pathways observed in Figure 8. As the entrance channel complex absorbs IR photons, the route taken across the reactive surface is dictated by the first channel to open. In the case of the $n = 8$ species, with its unpaired electron, this is TS1 between the entrance channel and the activated species, and further to complete dissociation and CO loss, an overall exothermic process. By contrast, on the $n = 9$ singlet surface, the dissociation channel to the $\text{Au}_9^+ + \text{OCS}$ asymptote opens below TS1 and thus this channel dominates. The size-selective IR-driven chemistry observed in Figure 8 is thus diagnostic of the differing shapes of the potential energy surface.

Similar arguments apply to all cluster sizes ($n = 2-10$) and Figure 11a) compares the relative energies of the three important $\text{Au}_n(\text{OCS})^+$ minima identified for $n = 8, 9$ in Figure 10, together with those of the $\text{Au}_n^+ + \text{OCS} / \text{Au}_n\text{S}^+ + \text{CO}$ thresholds. The geometries of these corresponding minima and relevant molecular orbitals are depicted in Figures S11, S13 and S14, in the supporting information. All cluster sizes have an S-bound entrance channel complex with binding energy reducing smoothly with increasing n , consistent with the reactivity data in Figure 2 (black columns). In contrast, the calculated energies of the activated species show clear separation between even and odd cluster sizes, with the former all significantly bound, unlike the odd cluster equivalents. This point is emphasised by the oscillation in Figure 11b).

The CO loss channel is only favourable if both: i) the overall process is exothermic, and ii) the barriers along the pathway are all submerged relative to the $\text{Au}_n^+ + \text{OCS}$ threshold. Within the uncertainty of the calculations, the overall $\text{Au}_n(\text{OCS})^+ \rightarrow \text{Au}_n\text{S}^+ + \text{CO}$ reaction (process 2) is thermodynamically possible for almost all even n clusters studied ($n = 4$ being the notable exception). Conversely, $n = 9$ is the only odd cluster with an exothermic pathway. Furthermore, although there is no spectroscopic evidence for the activated species, both TS1 and TS2 must, by

definition, lie higher in energy than the activated species. Hence, real barriers to reaction must exist on the $n = 3, 5$ and 9 surfaces (see also Figure 10). It is reasonable to assume that the barriers connecting the lower-lying minima associated with the even clusters will have lower transition states, similar to $n = 8$ (Figure 10).

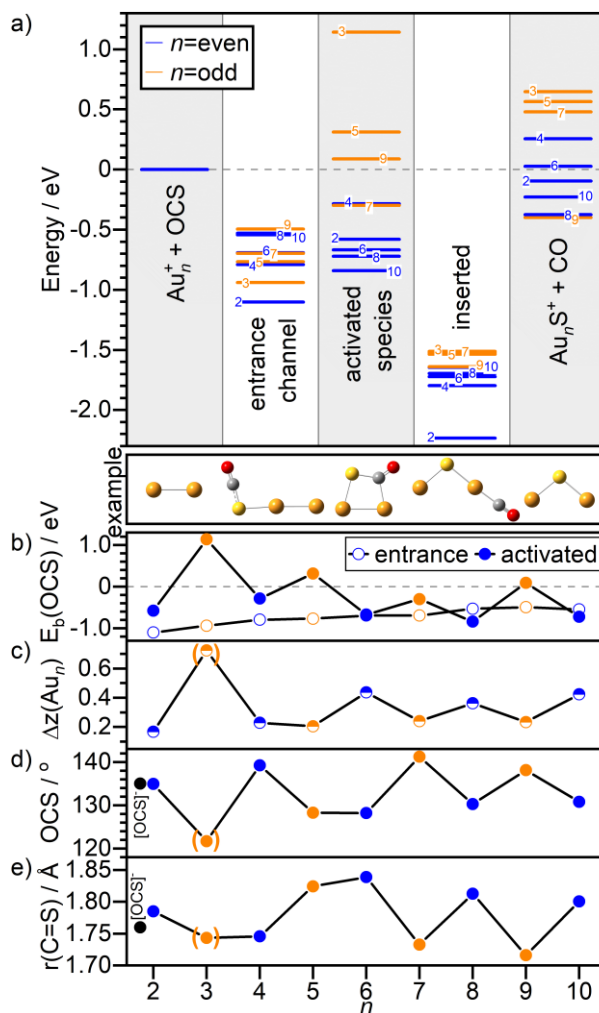


Figure 11. a) The minima on the potential energy surface of cluster sizes $n = 2-10$. It illustrates an odd-even effect – the unpaired electron in even cluster sizes is able to stabilise the activated species. The $\text{Au}_2(\text{OCS})^+$ series is given as example structure types. b) The binding energies of the spectrally assigned entrance channel species and the activated species relative to the $\text{Au}_n^+ + \text{OCS}$ asymptote. c) The difference in the Mulliken atomic charges located on Au_n in the activated and entrance channel species. d) The OCS bond angle in the activated species. e) The C=S bond length in the activated species. The

brackets for $n = 3$ indicate the different form of the activated species for this cluster, with the cluster base not intact.

The radical nature of Au_n^+ ($n = \text{even}$) clusters and closed-shell Au_n^+ ($n = \text{odd}$) are reflected in the respective doublet and singlet multiplicities of the ground state $\text{Au}_n(\text{OCS})^+$ surfaces. By analogy with CO_2 , an effective way of activating OCS is partial electron transfer into the antibonding LUMO orbital, which drives bending of the molecule.⁹⁵⁻⁹⁷ Although most common in anionic species,^{103, 124-126} Jiang and coworkers, and others have observed cationic clusters donating electron density for CO_2 activation,^{127 128} and Fielicke *et al.* described the ability of Au_n^+ to activate NO molecules.⁷ Hence, even though positively charged, the unpaired electron in the even n clusters is diffuse, weakly-bound, and readily donated (see Figure 11c). The opposite is true for the odd clusters (note that Au_3^+ has a qualitatively different activated species). Electron donation from closed-shell cationic clusters is highly unfavourable as shown in Figure 11c), resulting in reduced stabilisation of the activated species. Figure S13, in the supporting information shows an orbital representation of the electron donation for $n = 8$. In a similar way to that noted by Holmgren *et al.*,¹²⁹ the well matched symmetry of the Au_8^+ HOMO and OCS LUMO enhances their interaction. Figure 11 d)-e) illustrate structural parameters in the activated species (bond angles and bond lengths), demonstrating the degree of activation, which also show alternations.

The relevant calculated potential minima go some way to explaining the unusual observations made for $\text{Au}_5\text{S}(\text{OCS})^+$, in which absence of the C=S band (Figure 8) was assigned to dissociatively adsorbed OCS. Simulated spectra for $\text{Au}_5\text{S}(\text{OCS})^+$ isomers are depicted in Figure S9, supporting information. Figure 12b shows that the activated $\text{Au}_5\text{S}(\text{OCS})^+$ lies particularly low in energy, and so it is possible that the entrance channel species is not trapped at all. In this case, the fluxionality

around the central Au_5^+ atom facilitates surmounting TS1. Previously, low-energy intermediates were predicted only for even size clusters but the structures of $\text{Au}_5\text{S}(\text{OCS})^+$ are highly similar to the Au_6^+ pathway in Figure S11. It seems as if the sulfur atom behaves like an additional gold atom inducing a reversal in the odd-even electron counting effect for $n = 5$. In addition, Figure 12a shows significant enhancement into Au_5S_2^+ following $\text{Au}_5\text{S}(\text{OCS})^+$ excitation, which is also unique to this cluster size. The overall process in Figure 12b is endothermic, so when IR light is absorbed, the loss of CO and formation of Au_5S_2^+ is a higher energy process than OCS loss. However, if the OCS is indeed already dissociated then CO loss is more facile as OCS formation and loss would require a bimolecular surface reaction.

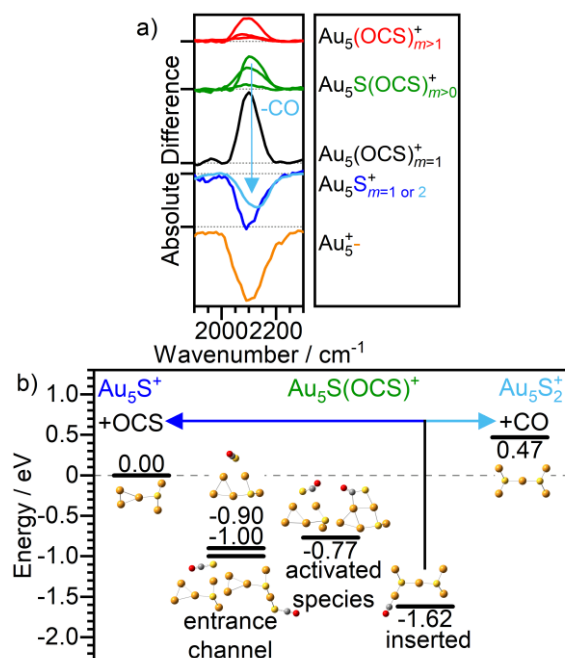


Figure 12. a) The IR-MPD spectra of $\text{Au}_5\text{S}_x(\text{OCS})_m^+$ in the region of the C=O stretch. Intensity is given as absolute difference (infrared on - infrared off), with depletion plotted in the positive direction. b) The minima on the potential energy surface of $\text{Au}_5\text{S}(\text{OCS})^+$

4. Summary and Conclusions

Infrared multiple photon dissociation spectroscopy combined with quantum chemical calculations has led to a detailed understanding of the nature of the binding of OCS to small gold cluster cations. Spectra are interpreted as the fundamental bands (and in some cases combination bands) of OCS vibrational modes. All evidence points to OCS being molecularly S-bound at atop sites on gold clusters in entrance channel minima, rather than the lowest energy, C=S inserted, structures. The only exception is the $n = 5$ cluster for which evidence of μ^2 binding exists due to the uniquely flexible bow tie structure of Au_5^+ .

Of particular note, marked odd-even alternations in the branching ratio for OCS vs CO loss are observed following pumping of the infrared OCS bands in $\text{Au}_n(\text{OCS})^+$. These fluctuations reflect the size-dependent features of the $\text{Au}_n^+ + \text{OCS} \rightarrow \text{Au}_n\text{S}^+ + \text{CO}$ reactive potential energy surface and mark the first time such alternating size-selective effects have been observed in infrared-driven cluster reactivity. Similar IR-driven chemistry on small metal clusters has previously been observed in the case of nitrous oxide decomposition on rhodium and rhodium oxide clusters ($[\text{Rh}_n\text{O}_m(\text{N}_2\text{O})]^{+/-}$)^{94, 121-122} and in the CO oxidation reaction on platinum oxide clusters ($[\text{Pt}_n\text{O}(\text{CO})]^+$).¹²⁰ In the former case, the fact that comparable chemistry was observed in subsequent collisional and black-body radiation experiments suggests a purely statistical (*i.e.*, thermal) process.¹³⁰⁻¹³¹ To the best of our knowledge, however, there have been no single collision experiments on the $\text{OCS} + \text{Au}_n^+$ reaction. It would be interesting to see if the odd-even alternation in the decomposition reaction observed here were preserved in such reactivity experiments.

ASSOCIATED CONTENT

Supporting Information.

See supporting information for further experimental data including IR-MPD spectra for all clusters and further computational information, simulated spectra and the supporting structures to the minima along the reaction pathways of all sizes.

AUTHOR INFORMATION

Corresponding Author

*stuart.mackenzie@chem.ox.ac.uk

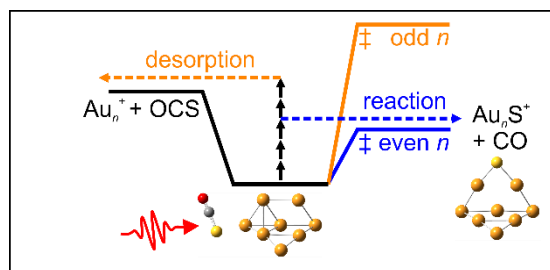
Author Contributions

The manuscript was written through contributions of all authors. All authors have given approval to the final version of the manuscript.

ACKNOWLEDGMENT

This work is funded by EPSRC under Programme Grant EP/L005913 and SCG Chemicals Co. via the Oxford Centre of Excellence Innovation Fund. AEG and GM thank Magdalen and Worcester Colleges, Oxford for their graduate studentships. AF thanks the Deutsche Forschungsgemeinschaft for a Heisenberg grant (FI 893/5).

TOC Graphic



REFERENCES

1. Hutchings, G. J., New directions in gold catalysis. *Gold Bull* **2004**, 37, 3-11.
2. Haruta, M., Catalysis: gold rush. *Nature* **2005**, 437, 1098-9.
3. Taketoshi, A.; Haruta, M., Size- and Structure-specificity in Catalysis by Gold Clusters. *Chem Lett* **2014**, 43 (4), 380-387.
4. Phala, N. S.; van Steen, E., Intrinsic reactivity of gold nanoparticles: Classical, semi-empirical and DFT studies. *Gold Bull* **2007**, 40, 150-153.
5. Pyykkö, P., Theoretical chemistry of gold. *Angew Chem Int Ed* **2004**, 43 (34), 4412-56.
6. Pyykkö, P., Theoretical chemistry of gold. II. *Inorg Chim Acta* **2005**, 358 (14), 4113-4130.
7. Fielicke, A.; von Helden, G.; Meijer, G.; Simard, B.; Rayner, D. M., Direct observation of size dependent activation of NO on gold clusters. *Phys Chem Chem Phys* **2005**, 7, 3906-9.
8. Haruta, M., Size- and support-dependency in the catalysis of gold. *Catal Today* **1997**, 36, 153-166.
9. Bond, G. C.; Thompson, D. T., Catalysis by gold. *Catal Rev Sci Eng* **1999**, 41 (3-4), 319-388.
10. Choudhary, T. V.; Goodman, D. W., Oxidation catalysis by supported gold nano-clusters. *Top Catal* **2002**, 21, 25-34.
11. Haruta, M., When gold is not noble: catalysis by nanoparticles. *Chem Rec* **2003**, 3 (2), 75-87.
12. Wallace, W. T.; Wyrwas, R. B.; Whetten, R. L.; Mitrić, R.; Bonačić-Koutecký, V., Oxygen adsorption on hydrated gold cluster anions: experiment and theory. *J Am Chem Soc* **2003**, 125 (27), 8408-14.
13. Ding, Z.; Yan, L.; Li, Z.; Ma, W.; Lu, G.; Meng, S., Controlling catalytic activity of gold cluster on MgO thin film for water splitting. *Phys Rev Mater* **2017**, 1 (4), 045404.
14. Dubois, L. H.; Nuzzo, R. G., Synthesis, Structure, and Properties of Model Organic Surfaces. *Annu Rev Phys Chem* **1992**, 43, 437-463.
15. Ulman, A., Formation and Structure of Self-Assembled Monolayers. *Chem Rev* **1996**, 96 (4), 1533-1554.
16. Sugawara, K.-i.; Sobott, F.; Vakhtin, A. B., Reactions of gold cluster cations Au_n^+ ($n=1-12$) with H_2S and H_2 . *J Chem Phys* **2003**, 118, 7808-7816.
17. Pei, Y.; Zeng, X. C., Investigating the structural evolution of thiolate protected gold clusters from first-principles. *Nanoscale* **2012**, 4, 4054-72.
18. Häkkinen, H., The gold-sulfur interface at the nanoscale. *Nat Chem* **2012**, 4, 443-55.
19. Jadzinsky, P. D.; Calero, G.; Ackerson, C. J.; Bushnell, D. A.; Kornberg, R. D., Structure of a thiol monolayer-protected gold nanoparticle at 1.1 Å resolution. *Science* **2007**, 318 (5849), 430-3.

20. Veldeman, N.; Lievens, P.; Andersson, M., Size-dependent carbon monoxide adsorption on neutral gold clusters. *J Phys Chem A* **2005**, *109* (51), 11793-801.
21. Haruta, M.; Yamada, N.; Kobayashi, T.; Iijima, S., Gold Catalysts Prepared by Coprecipitation for Low-Temperature Oxidation of Hydrogen and of Carbon-Monoxide. *J Catal* **1989**, *115* (2), 301-309.
22. Zhu, Y.; Jin, R.; Sun, Y., Atomically Monodisperse Gold Nanoclusters Catalysts with Precise Core-Shell Structure. *Catalysts* **2011**, *1* (1), 3-17.
23. Zhang, Y.; Song, P.; Chen, T.; Liu, X.; Chen, T.; Wu, Z.; Wang, Y.; Xie, J.; Xu, W., Unique size-dependent nanocatalysis revealed at the single atomically precise gold cluster level. *Proc Natl Acad Sci U S A* **2018**, *115* (42), 10588-10593.
24. Valden, M.; Lai, X.; Goodman, D. W., Onset of catalytic activity of gold clusters on titania with the appearance of nonmetallic properties. *Science* **1998**, *281* (5383), 1647-50.
25. Wu, X.; Senapati, L.; Nayak, S. K.; Selloni, A.; Hajaligol, M., A density functional study of carbon monoxide adsorption on small cationic, neutral, and anionic gold clusters. *J Chem Phys* **2002**, *117*, 4010-4015.
26. Yoon, B.; Häkkinen, H.; Landman, U.; Wörz, A. S.; Antonietti, J. M.; Abbet, S.; Judai, K.; Heiz, U., Charging effects on bonding and catalyzed oxidation of CO on Au₈ clusters on MgO. *Science* **2005**, *307* (5708), 403-7.
27. Sanchez, A.; Abbet, S.; Heiz, U.; Schneider, W. D.; Häkkinen, H.; Barnett, R. N.; Landman, U., When Gold Is Not Noble: Nanoscale Gold Catalysts. *J Phys Chem A* **1999**, *103* (48), 9573-9578.
28. Guzman, J.; Gates, B. C., Simultaneous presence of cationic and reduced gold in functioning MgO-supported CO oxidation catalysts: Evidence from X-ray absorption spectroscopy. *J Phys Chem B* **2002**, *106* (31), 7659-7665.
29. Guzman, J.; Gates, B. C., Catalysis by supported gold: correlation between catalytic activity for CO oxidation and oxidation states of gold. *J Am Chem Soc* **2004**, *126* (9), 2672-3.
30. Hutchings, G. J.; Hall, M. S.; Carley, A. F.; Landon, P.; Solsona, B. E.; Kiely, C. J.; Herzing, A.; Makkee, M.; Moulijn, J. A.; Overweg, A., *et al.*, Role of gold cations in the oxidation of carbon monoxide catalyzed by iron oxide-supported gold. *J Catal* **2006**, *242* (1), 71-81.
31. Böhme, D. K.; Schwarz, H., Gas-phase catalysis by atomic and cluster metal ions: the ultimate single-site catalysts. *Angew Chem Int Ed* **2005**, *44* (16), 2336-54.
32. Lang, S. M.; Bernhardt, T. M., Gas phase metal cluster model systems for heterogeneous catalysis. *Phys Chem Chem Phys* **2012**, *14*, 9255-69.
33. Bernhardt, T.; Heiz, U.; Landman, U., Chemical and Catalytic Properties of Size-Selected Free and Supported Clusters. In *Nanocatalysis. Nanoscience and Technology*, Heiz, U.; Landman, U., Eds. Springer Berlin Heidelberg: Berlin, Heidelberg, 2007; pp 1-191.
34. Johansson, M. P.; Lechtken, A.; Schooss, D.; Kappes, M. M.; Furche, F., 2D-3D transition of gold cluster anions resolved. *Phys Rev A* **2008**, *77* (5), 053202.
35. Goldsmith, B. R.; Florian, J.; Liu, J. X.; Gruene, P.; Lyon, J. T.; Rayner, D. M.; Fielicke, A.; Scheffler, M.; Ghiringhelli, L. M., Two-to-three dimensional transition in neutral gold clusters: The crucial role of van der Waals interactions and temperature. *Phys Rev Mater* **2019**, *3* (1), 016002.

36. Häkkinen, H.; Yoon, B.; Landman, U.; Li, X.; Zhai, H.-J.; Wang, L.-S., On the Electronic and Atomic Structures of Small Au_N^- ($N=4-14$) Clusters: A Photoelectron Spectroscopy and Density-Functional Study. *J Phys Chem A* **2003**, *107* (32), 6168-6175.
37. Weis, P.; Bierweiler, T.; Vollmer, E.; Kappes, M. M., Au_9^+ : Rapid isomerization reactions at 140 K. *J Chem Phys* **2002**, *117*, 9293-9297.
38. Gilb, S.; Weis, P.; Furche, F.; Ahlrichs, R.; Kappes, M. M., Structures of small gold cluster cations (Au_n^+ , $n<14$): Ion mobility measurements versus density functional calculations. *J Chem Phys* **2002**, *116*, 4094-4101.
39. Furche, F.; Ahlrichs, R.; Weis, P.; Jacob, C.; Gilb, S.; Bierweiler, T.; Kappes, M. M., The structures of small gold cluster anions as determined by a combination of ion mobility measurements and density functional calculations. *J Chem Phys* **2002**, *117*, 6982-6990.
40. Gloess, A. N.; Schneider, H.; Weber, J. M.; Kappes, M. M., Electronically excited states and visible region photodissociation spectroscopy of $\text{Au}_m^+ \cdot \text{Ar}_n$ clusters ($m=7-9$): molecular dimensionality transition? *J Chem Phys* **2008**, *128*, 114312.
41. Gibson, J. K., Laser ablation and gas-phase reactions of small gold cluster ions, Au_n^+ ($1 \leq n \leq 7$). *J Vac Sci Technol A* **1998**, *16*, 653-659.
42. Herlert, A.; Krückeberg, S.; Schweikhard, L.; Vogel, M.; Walther, C., Electron impact ionization/dissociation of size selected gold cluster cations. *J Electron Spectrosc Relat Phenom* **2000**, *106* (2-3), 179-186.
43. Becker, S.; Dietrich, G.; Hasse, H. U.; Klisch, N.; Kluge, H. J.; Kreisle, D.; Krückeberg, S.; Lindinger, M.; Lützenkirchen, K.; Schweikhard, L., *et al.*, Collision Induced Dissociation of Stored Gold Cluster Ions. *Z Phys D: At, Mol Clusters* **1994**, *30*, 341-348.
44. Katakuse, I.; Ichihara, T.; Fujita, Y.; Matsuo, T.; Sakurai, T.; Matsuda, H., Mass Distributions of Copper, Silver and Gold Clusters and Electronic Shell Structure. *Int J Mass Spectrom Ion Processes* **1985**, *67* (2), 229-236.
45. Veldeman, N.; Janssens, E.; Hansen, K.; De Haeck, J.; Silverans, R. E.; Lievens, P., Stability and dissociation pathways of doped Au_nX^+ clusters ($\text{X} = \text{Y}, \text{Er}, \text{Nb}$). *Faraday Discuss* **2008**, *138*, 147-62.
46. Ferrari, P.; Hussein, H. A.; Heard, C. J.; Vanbuel, J.; Johnston, R. L.; Lievens, P.; Janssens, E., Effect of palladium doping on the stability and fragmentation patterns of cationic gold clusters. *Phys Rev A* **2018**, *97* (5), 052508.
47. Hansen, K.; Ferrari, P.; Janssens, E.; Lievens, P., Thermal radiation of gold clusters on microsecond time scales. *Phys Rev A* **2017**, *96* (2), 022511.
48. Häkkinen, H., Atomic and electronic structure of gold clusters: understanding flakes, cages and superatoms from simple concepts. *Chem Soc Rev* **2008**, *37*, 1847-59.
49. Knickelbein, M. B., Reactions of transition metal clusters with small molecules. *Annu Rev Phys Chem* **1999**, *50*, 79-115.
50. Knight, W. D.; Clemenger, K.; de Heer, W. A.; Saunders, W. A.; Chou, M. Y.; Cohen, M. L., Electronic Shell Structure and Abundances of Sodium Clusters. *Phys Rev Lett* **1984**, *52* (24), 2141-2143.
51. Koskinen, M.; Lipas, P. O.; Manninen, M., Electron-Gas Clusters - the Ultimate Jellium Model. *Z Phys D: At, Mol Clusters* **1995**, *35*, 285-297.

52. Ekardt, W., Work Function of Small Metal Particles: Self-Consistent Spherical Jellium-Background Model. *Phys Rev B* **1984**, 29 (4), 1558-1564.
53. de Heer, W. A., The physics of simple metal clusters: experimental aspects and simple models. *Rev Mod Phys* **1993**, 65 (3), 611-676.
54. Salisbury, B. E.; Wallace, W. T.; Whetten, R. L., Low-temperature activation of molecular oxygen by gold clusters: a stoichiometric process correlated to electron affinity. *Chem Phys* **2000**, 262 (1), 131-141.
55. Yoon, B.; Koskinen, P.; Huber, B.; Kostko, O.; von Issendorff, B.; Häkkinen, H.; Moseler, M.; Landman, U., Size-dependent structural evolution and chemical reactivity of gold clusters. *ChemPhysChem* **2007**, 8, 157-61.
56. Yoon, B.; Häkkinen, H.; Landman, U., Interaction of O₂ with Gold Clusters: Molecular and Dissociative Adsorption. *J Phys Chem A* **2003**, 107 (20), 4066-4071.
57. Bernhardt, T. M., Gas-phase kinetics and catalytic reactions of small silver and gold clusters. *Int J Mass Spectrom* **2005**, 243 (1), 1-29.
58. Woodham, A. P.; Fielicke, A., Gold Clusters in the Gas Phase. In *Gold Clusters, Colloids and Nanoparticles I. Structure and Bonding*, Mingos, D., Ed. Springer, Cham: Berlin Heidelberg, 2013; Vol. 161.
59. Huang, W.; Zhai, H. J.; Wang, L. S., Probing the interactions of O₂ with small gold cluster anions (Au_n⁻, n = 1-7): chemisorption vs physisorption. *J Am Chem Soc* **2010**, 132 (12), 4344-51.
60. Pal, R.; Wang, L. M.; Pei, Y.; Wang, L. S.; Zeng, X. C., Unraveling the mechanisms of O₂ activation by size-selected gold clusters: transition from superoxo to peroxo chemisorption. *J Am Chem Soc* **2012**, 134 (22), 9438-45.
61. Lee, T. H.; Ervin, K. M., Reactions of Copper Group Cluster Anions with Oxygen and Carbon Monoxide. *J Phys Chem-Us* **1994**, 98 (40), 10023-10031.
62. Lang, S. M.; Bernhardt, T. M.; Barnett, R. N.; Yoon, B.; Landman, U., Hydrogen-promoted oxygen activation by free gold cluster cations. *J Am Chem Soc* **2009**, 131 (25), 8939-51.
63. Woodham, A. P.; Meijer, G.; Fielicke, A., Activation of molecular oxygen by anionic gold clusters. *Angew Chem Int Ed* **2012**, 51 (18), 4444-7.
64. Woodham, A. P.; Fielicke, A., Superoxide formation on isolated cationic gold clusters. *Angew Chem Int Ed* **2014**, 53 (25), 6554-7.
65. Woodham, A. P.; Meijer, G.; Fielicke, A., Charge separation promoted activation of molecular oxygen by neutral gold clusters. *J Am Chem Soc* **2013**, 135 (5), 1727-30.
66. Fielicke, A.; von Helden, G.; Meijer, G.; Pedersen, D. B.; Simard, B.; Rayner, D. M., Gold cluster carbonyls: saturated adsorption of CO on gold cluster cations, vibrational spectroscopy, and implications for their structures. *J Am Chem Soc* **2005**, 127 (23), 8416-23.
67. Lang, S. M.; Bernhardt, T. M.; Chernyy, V.; Bakker, J. M.; Barnett, R. N.; Landman, U., Selective C-H Bond Cleavage in Methane by Small Gold Clusters. *Angew Chem Int Ed Engl* **2017**, 56 (43), 13406-13410.
68. Knickelbein, M. B.; Koretsky, G. M., Infrared Studies of the Interaction of Methanol with Cu_n, Ag_n, and Au_n. *J Phys Chem A* **1998**, 102 (3), 580-586.

69. Dietrich, G.; Krückeberg, S.; Lützenkirchen, K.; Schweikhard, L.; Walther, C., The interaction of gold clusters with methanol molecules: Infrared photodissociation of mass-selected $\text{Au}_n^+(\text{CH}_3\text{OH})_m$. *J Chem Phys* **2000**, *112* (2), 752-760.
70. Rousseau, R.; Marx, D., The interaction of gold clusters with methanol molecules: Ab initio molecular dynamics of $\text{Au}_n^+\text{CH}_3\text{OH}$ and $\text{Au}_n\text{CH}_3\text{OH}$. *J Chem Phys* **2000**, *112*, 761-769.
71. Koretsky, G. M.; Knickelbein, M. B.; Rousseau, R.; Marx, D., A combined infrared photodissociation and theoretical study of the interaction of ethanol with small gold clusters. *J Phys Chem A* **2001**, *105* (50), 11197-11203.
72. Lang, S. M.; Bernhardt, T. M.; Bakker, J. M.; Yoon, B.; Landman, U., The interaction of ethylene with free gold cluster cations: infrared photodissociation spectroscopy combined with electronic and vibrational structure calculations. *J Phys Condens Matter* **2018**, *30* (50), 504001.
73. Lang, S. M.; Bernhardt, T. M.; Barnett, R. N.; Landman, U., Size-dependent binding energies of methane to small gold clusters. *ChemPhysChem* **2010**, *11* (7), 1570-7.
74. Cunningham, E. M.; Gentleman, A. S.; Beardsmore, P. W.; Iskra, A.; Mackenzie, S. R., Infrared Signature of Structural Isomers of Gas-Phase $\text{M}^+(\text{N}_2\text{O})_n$ ($\text{M} = \text{Cu}, \text{Ag}, \text{Au}$) Ion-Molecule Complexes. *J Phys Chem A* **2017**, *121* (40), 7565-7571.
75. Velasquez, J.; Njegic, B.; Gordon, M. S.; Duncan, M. A., IR photodissociation spectroscopy and theory of $\text{Au}^+(\text{CO})_n$ complexes: nonclassical carbonyls in the gas phase. *J Phys Chem A* **2008**, *112* (9), 1907-13.
76. Li, Y.; Wang, G.; Wang, C.; Zhou, M., Coordination and solvation of the Au^+ cation: infrared photodissociation spectroscopy of mass-selected $\text{Au}(\text{H}_2\text{O})_n^+$ ($n = 1-8$) complexes. *J Phys Chem A* **2012**, *116* (44), 10793-801.
77. Li, Y.; Wang, L.; Qu, H.; Wang, G.; Zhou, M., Infrared photodissociation spectroscopy of mass-selected silver and gold nitrosyl cation complexes. *J Phys Chem A* **2015**, *119* (15), 3577-86.
78. Ward, T. B.; Brathwaite, A. D.; Duncan, M. A., Infrared Spectroscopy of $\text{Au}(\text{Acetylene})_n^+$ Complexes in the Gas Phase. *Top Catal* **2018**, *61*, 49-61.
79. Gentleman, A. S.; Green, A. E.; Price, D. R.; Cunningham, E. M.; Iskra, A.; Mackenzie, S. R., Infrared Spectroscopy of $\text{Au}^+(\text{CH}_4)_n$ Complexes and Vibrationally-Enhanced C-H Activation Reactions. *Top Catal* **2018**, *61* (1), 81-91.
80. Häkkinen, H.; Landman, U., Gas-phase catalytic oxidation of CO by Au_2^- . *J Am Chem Soc* **2001**, *123* (39), 9704-5.
81. Wallace, W. T.; Whetten, R. L., Coadsorption of CO and O_2 on selected gold clusters: evidence for efficient room-temperature CO_2 generation. *J Am Chem Soc* **2002**, *124* (25), 7499-505.
82. Hagen, J.; Socaciu, L. D.; Elijażyfer, M.; Heiz, U.; Bernhardt, T. M.; Wöste, L., Coadsorption of CO and O_2 on small free gold cluster anions at cryogenic temperatures: Model complexes for catalytic CO oxidation. *Phys Chem Chem Phys* **2002**, *4*, 1707-1709.
83. Yuan, D. W.; Zeng, Z., Saturated adsorption of CO and coadsorption of CO and O_2 on Au_N^- ($N=2-7$) clusters. *J Chem Phys* **2004**, *120* (4), 6574-84.
84. Rue, C.; Armentrout, P. B.; Kretzschmar, I.; Schröder, D.; Schwarz, H., Guided ion beam studies of the state-specific reactions of Cr^+ and Mn^+ with CS_2 and COS . *Int J Mass Spectrom* **2001**, *210*, 283-301.

85. Armentrout, P. B.; Cox, R. M.; Sweeny, B. C.; Ard, S. G.; Shuman, N. S.; Viggiano, A. A., Lanthanides as Catalysts: Guided Ion Beam and Theoretical Studies of $\text{Sm}^+ + \text{COS}$. *J Phys Chem A* **2018**, *122* (3), 737-749.
86. Rue, C.; Armentrout, P. B.; Kretzschmar, I.; Schröder, D.; Schwarz, H., Guided ion beam studies of the reactions of Ni^+ , Cu^+ , and Zn^+ with CS_2 and COS . *J Phys Chem A* **2002**, *106* (42), 9788-9797.
87. Rue, C.; Armentrout, P. B.; Kretzschmar, I.; Schröder, D.; Schwarz, H., Guided ion beam studies of the reactions of Fe^+ and Co^+ with CS_2 and COS . *J Phys Chem A* **2001**, *105* (37), 8456-8464.
88. Kretzschmar, I.; Schröder, D.; Schwarz, H.; Rue, C.; Armentrout, P. B., Experimental and theoretical studies of vanadium sulfide cation. *J Phys Chem A* **1998**, *102* (49), 10060-10073.
89. Kretzschmar, I.; Schröder, D.; Schwarz, H.; Rue, C.; Armentrout, P. B., Thermochemistry and reactivity of cationic scandium and titanium sulfide in the gas phase. *J Phys Chem A* **2000**, *104* (21), 5046-5058.
90. Blagojevic, V.; Lavrov, V. V.; Bohme, D. K., Ligation kinetics as a probe for relativistic effects in ion chemistry: Gas-phase ligation of late atomic transition metal cations with OCS and CH_3Cl at room temperature. *Int J Mass Spectrom* **2018**, *429*, 101-106.
91. Svoronos, P. D. N.; Bruno, T. J., Carbonyl sulfide: A review of its chemistry and properties. *Ind Eng Chem Res* **2002**, *41* (22), 5321-5336.
92. Wang, X.; Qiu, J.; Ning, P.; Ren, X.; Li, Z.; Yin, Z.; Chen, W.; Liu, W., Adsorption/desorption of low concentration of carbonyl sulfide by impregnated activated carbon under micro-oxygen conditions. *J Hazard Mater* **2012**, *229-230*, 128-36.
93. Sass, C. S.; Rabalais, J. W., Chemisorption of Carbonyl Sulfide (OCS) on Ni between 77 K and 293 K. *Surf Sci* **1988**, *194*, L95-L99.
94. Hamilton, S. M.; Hopkins, W. S.; Harding, D. J.; Walsh, T. R.; Gruene, P.; Haertelt, M.; Fielicke, A.; Meijer, G.; Mackenzie, S. R., Infrared induced reactivity on the surface of isolated size-selected clusters: dissociation of N_2O on rhodium clusters. *J Am Chem Soc* **2010**, *132* (5), 1448-9.
95. McBane, G. C.; Schmidt, J. A.; Johnson, M. S.; Schinke, R., Ultraviolet photodissociation of OCS : product energy and angular distributions. *J Chem Phys* **2013**, *138*, 094314.
96. Walsh, A. D., The Electronic Orbitals, Shapes, and Spectra of Polyatomic Molecules . Part II. Non-Hydride AB_2 and BAC Molecules. *J Chem Soc* **1953**, 2266-2288.
97. Buenker, R. J.; Peyerimhoff, S. D., Molecular geometry and the Mulliken-Walsh molecular orbital model. An ab initio study. *Chem Rev* **1974**, *74* (2), 127-188.
98. Iskra, A.; Gentleman, A. S.; Kartouzian, A.; Kent, M. J.; Sharp, A. P.; Mackenzie, S. R., Infrared Spectroscopy of Gas-Phase $\text{M}^+(\text{CO}_2)_n$ ($\text{M} = \text{Co}, \text{Rh}, \text{Ir}$) Ion-Molecule Complexes. *J Phys Chem A* **2017**, *121* (1), 133-140.
99. Zhao, Z.; Kong, X.; Yang, D.; Yuan, Q.; Xie, H.; Fan, H.; Zhao, J.; Jiang, L., Reactions of Copper and Silver Cations with Carbon Dioxide: An Infrared Photodissociation Spectroscopic and Theoretical Study. *J Phys Chem A* **2017**, *121* (17), 3220-3226.

100. Duncan, M. A., Infrared spectroscopy to probe structure and dynamics in metal ion-molecule complexes. *Int Rev Phys Chem* **2003**, 22 (2), 407-435.
101. Walker, N. R.; Walters, R. S.; Duncan, M. A., Frontiers in the infrared spectroscopy of gas phase metal ion complexes. *New J Chem* **2005**, 29, 1495-1503.
102. Xing, X. p.; Wang, G. j.; Wang, C. x.; Zhou, M. f., Infrared Photodissociation Spectroscopy of $\text{Ti}^+(\text{CO}_2)_2\text{Ar}$ and $\text{Ti}^+(\text{CO}_2)_n$ ($n=3-7$) Complexes. *Chin J Chem Phys* **2013**, 26 (6), 687-693.
103. Weber, J. M., The interaction of negative charge with carbon dioxide - insight into solvation, speciation and reductive activation from cluster studies. *Int Rev Phys Chem* **2014**, 33 (4), 489-519.
104. Green, A. E.; Justen, J.; Schöllkopf, W.; Gentleman, A. S.; Fielicke, A.; Mackenzie, S. R., IR Signature of Size-Selective CO_2 Activation on Small Platinum Cluster Anions, Pt_n^- ($n=4-7$). *Angew Chem Int Ed* **2018**, 57 (45), 14822-14826.
105. Schöllkopf, W.; Gewinner, S.; Junkes, H.; Paarmann, A.; von Helden, G.; Bluem, H.; Todd, A. M. M., The new IR and THz FEL facility at the Fritz Haber Institute in Berlin. *Proc. SPIE* **2015**, 9512, 95121L.
106. Yanagimachi, A.; Koyasu, K.; Valdivielso, D. Y.; Gewinner, S.; Schöllkopf, W.; Fielicke, A.; Tsukuda, T., Size-Specific, Dissociative Activation of Carbon Dioxide by Cobalt Cluster Anions. *J Phys Chem C* **2016**, 120 (26), 14209-14215.
107. Truong, N. X.; Haertelt, M.; Jaeger, B. K. A.; Gewinner, S.; Schöllkopf, W.; Fielicke, A.; Dopfer, O., Characterization of neutral boron-silicon clusters using infrared spectroscopy: The case of Si_6B . *Int J Mass Spectrom* **2016**, 395, 1-6.
108. Addicoat, M. A.; Metha, G. F., Kick: constraining a stochastic search procedure with molecular fragments. *J Comput Chem* **2009**, 30, 57-64.
109. Perdew, J. P., Density-functional approximation for the correlation energy of the inhomogeneous electron gas. *Phys Rev B* **1986**, 33 (12), 8822-8824.
110. Andrae, D.; Häußermann, U.; Dolg, M.; Stoll, H.; Preuß, H., Energy-Adjusted Ab Initio Pseudopotentials for the Second and Third Row Transition Elements. *Theor Chim Acta* **1990**, 77, 123-141.
111. Perdew, J. P.; Tao, J.; Staroverov, V. N.; Scuseria, G. E., Meta-generalized gradient approximation: explanation of a realistic nonempirical density functional. *J Chem Phys* **2004**, 120 (15), 6898-911.
112. Weigend, F.; Ahlrichs, R., Balanced basis sets of split valence, triple zeta valence and quadruple zeta valence quality for H to Rn: Design and assessment of accuracy. *Phys Chem Chem Phys* **2005**, 7 (18), 3297-305.
113. Weigend, F., Accurate Coulomb-fitting basis sets for H to Rn. *Phys Chem Chem Phys* **2006**, 8, 1057-65.
114. Grimme, S.; Antony, J.; Ehrlich, S.; Krieg, H., A consistent and accurate ab initio parametrization of density functional dispersion correction (DFT-D) for the 94 elements H-Pu. *J Chem Phys* **2010**, 132, 154104.
115. Grimme, S.; Ehrlich, S.; Goerigk, L., Effect of the damping function in dispersion corrected density functional theory. *J Comput Chem* **2011**, 32 (7), 1456-65.
116. Shimanouchi, T., *Tables of Molecular Vibrational Frequencies Consolidated Volume I*. Nat. Stand. Ref. Data Ser., Nat. Bur. Stand.: Washington, D. C., 1972; Vol. 1.

117. Frisch, M. J.; Trucks, G. W.; Schlegel, H. B.; Scuseria, G. E.; Robb, M. A.; Cheeseman, J. R.; Scalmani, G.; Barone, V.; Mennucci, B.; Petersson, G. A., *et al.* *Gaussian 09, Revision D.01*, Gaussian, Inc.: Wallingford CT, 2013.
118. Darwent, B. d., *Bond Dissociation Energies in Simple Molecules*. Nat. Stand. Ref. Data Ser., Nat. Bur. Stand.: Washington, D. C., 1970; Vol. 31.
119. Lyalin, A.; Taketsugu, T., Cooperative Adsorption of O₂ and C₂H₄ on Small Gold Clusters. *J Phys Chem C* **2009**, *113* (30), 12930-12934.
120. Hermes, A. C.; Hamilton, S. M.; Cooper, G. A.; Kerpál, C.; Harding, D. J.; Meijer, G.; Fielicke, A.; Mackenzie, S. R., Infrared driven CO oxidation reactions on isolated platinum cluster oxides, Pt_nO_m⁺. *Faraday Discuss* **2012**, *157*, 213-25.
121. Hermes, A. C.; Hamilton, S. M.; Hopkins, W. S.; Harding, D. J.; Kerpál, C.; Meijer, G.; Fielicke, A.; Mackenzie, S. R., Effects of Coadsorbed Oxygen on the Infrared Driven Decomposition of N₂O on Isolated Rh₅⁺ Clusters. *J Phys Chem Lett* **2011**, *2* (24), 3053-3057.
122. Hamilton, S. M.; Hopkins, W. S.; Harding, D. J.; Walsh, T. R.; Haertelt, M.; Kerpál, C.; Gruene, P.; Meijer, G.; Fielicke, A.; Mackenzie, S. R., Infrared-induced reactivity of N₂O on small gas-phase rhodium clusters. *J Phys Chem A* **2011**, *115* (12), 2489-97.
123. Harding, D. J.; Kerpál, C.; Meijer, G.; Fielicke, A., Activated methane on small cationic platinum clusters. *Angew Chem Int Ed* **2012**, *51* (3), 817-9.
124. Thompson, M. C.; Ramsay, J.; Weber, J. M., Interaction of CO₂ with Atomic Manganese in the Presence of an Excess Negative Charge Probed by Infrared Spectroscopy of [Mn(CO₂)_n]⁻ Clusters. *J Phys Chem A* **2017**, *121* (40), 7534-7542.
125. Thompson, M. C.; Dodson, L. G.; Weber, J. M., Structural Motifs of [Fe(CO₂)_n]⁻ Clusters (n = 3-7). *J Phys Chem A* **2017**, *121* (21), 4132-4138.
126. Knurr, B. J.; Weber, J. M., Structural diversity of copper-CO₂ complexes: infrared spectra and structures of [Cu(CO₂)_n]⁻ clusters. *J Phys Chem A* **2014**, *118* (44), 10246-51.
127. Zhao, Z.; Kong, X.; Yuan, Q.; Xie, H.; Yang, D.; Zhao, J.; Fan, H.; Jiang, L., Coordination-induced CO₂ fixation into carbonate by metal oxides. *Phys Chem Chem Phys* **2018**, *20*, 19314-19320.
128. Ricks, A. M.; Brathwaite, A. D.; Duncan, M. A., IR spectroscopy of gas phase V(CO₂)_n⁺ clusters: solvation-induced electron transfer and activation of CO₂. *J Phys Chem A* **2013**, *117* (45), 11490-8.
129. Holmgren, L.; Grönbeck, H.; Andersson, M.; Rosén, A., CO on copper clusters: Orbital symmetry rules. *Phys Rev B* **1996**, *53* (24), 16644-16651.
130. Parry, I. S.; Kartouzian, A.; Hamilton, S. M.; Balaj, O. P.; Beyer, M. K.; Mackenzie, S. R., Collisional activation of N₂O decomposition and CO oxidation reactions on isolated rhodium clusters. *J Phys Chem A* **2013**, *117* (36), 8855-63.
131. Parry, I. S.; Kartouzian, A.; Hamilton, S. M.; Balaj, O. P.; Beyer, M. K.; Mackenzie, S. R., Chemical reactivity on gas-phase metal clusters driven by blackbody infrared radiation. *Angew Chem Int Ed* **2015**, *54* (4), 1357-60.